Materials Today Communications 39 (2024) 108987

Contents lists available at ScienceDirect

Materials Today Communications

journal homepage: www.elsevier.com/locate/mtcomm

Impact of thermal activation on the growth dynamics of thermoelastic martensitic transformation

K. Niitsu

National Institute for Materials Science, Tsukuba 305-0047, Japan

ARTICLE INFO

Keywords:
Shape memory alloys (SMA)
Interface dynamics
Thermally activated processes
Martensitic phase transformation
Phase transformation kinetics

ABSTRACT

The dynamics of thermoelastic martensitic transformations (MTs) become not straightforward with lowering temperatures due to the manifestation of the thermal activation process. The author recently proposed a new concept of "viscosuperelasticity" of which mathematical expression for the thermal activation of habit plane motion enables to quantitatively reproduce the MT dynamics under both the isothermal and anisothermal (dynamic cooling/heating) conditions. In this study, the time-dependent evolution of MTs is evaluated with the concept of viscosuperelasticity for some representative cases of MT-hosting alloy systems. This concept enables seemingly strange low-temperature behaviors to be explained as manifestations of thermal activation. Furthermore, undiscovered exceptional dynamics are also predicted to occur. This study guides the way to manifest the impact of time from experimentally accessible MT behaviors and provides a systematic understanding of low-temperature MT dynamics.

1. Introduction

Low-temperature dynamics of the thermoelastic martensitic transformation (MT) is not simple. After the discovery of the isothermal MT in Fe–Mn–C [1] and Fe–Ni–Mn alloys [2], this peculiar behavior has been studied for various MT-hosting alloy systems and has been regarded as a long-standing mystery underlying the fundamental mechanism of MT [3–6]. Before introducing the phenomenology of isothermal MTs, an overview of the kinetics and microstructural evolutions of MTs shall be mentioned.

Like many other 1st-order structural phase transformations, MT evolves by nucleation and growth with a finite hysteresis for dragging the transformation interfaces called habit planes. The kinetics of nucleation and growth involves both athermal and thermal natures [3–6]. Athermal dynamics depend on intensive variables such as temperature, stresses, magnetic fields, and chemical potential. In contrast, isothermal (thermally activated) dynamics depend on time along with the aforementioned intensive variables and are more pronounced at lower temperatures where thermal excitations are stochastically suppressed [7]. These two natures should be independently considered for nucleation and growth, the processes by which MTs develop.

The significance of nucleation and growth processes is different depending on which intensive variables trigger MT. Thermally- and magnetically-induced forward MTs give rise to multivariant martensitic microstructures, wherein burst-like nucleation and (at least macroscopically) smooth growth are involved [8,9]. In these situations, the evolution of MT is sometimes detected as a stepwise change superposed on the baseline bending of the measurands (for example, see Fig. 1 in ref. 10). Such stepwise behavior is less pronounced in reverse MT, and such nonreciprocal behavior between forward and reverse MTs is observable especially at decreased temperatures. This suggests, for thermally- and magnetically-induced MTs, the significance of nucleation and growth is not equivalent for forward and reverse pathways. Unlike such intricate dynamics of thermally- and magnetically-induced MTs, somewhat a simpler picture is applicable to stress-induced MTs. Generally, a limited number (ideally one) of variant(s) are introduced by application of uniaxial stress and are continuously expanded/contracted by further loading/unloading [11]. In such a situation, the role of nucleation is less pronounced, resulting in a smooth, parallel-piped superelastic stress-strain curve down to cryogenic temperatures (for example, see Fig. 2 in ref. 12).

The isothermal nature of the nucleation and growth processes has been identified as the key to describing the low-temperature isothermal dynamics of MTs [8,9,13–19]. Most of the isothermal studies have been performed on thermally- or magnetically-induced MTs, but considering the above-mentioned complexity, it may be challenging to resolve their respective isothermal/athermal nature of nucleation and growth dynamics. Assuming that the nucleation process in stress-induced MTs is

E-mail address: NIITSU.Kodai@nims.go.jp.

https://doi.org/10.1016/j.mtcomm.2024.108987
Received 29 December 2023; Received in revised form 15 April 2024; Accepted 20 April 2024
Available online 21 April 2024

negligible, analyzing the dynamics of stress-induced MTs is a promising way to access the athermal and isothermal nature of growth.

Recently, the author elucidated the isothermal growth dynamics of stress-induced forward and reverse MTs and proposed a mathematical model for thermal activation of the habit plane motion with the concept of viscosuperelasticity [20]. This concept claims that the following expression prescribes how the overloading/underloading stress required to drive the forward/reverse MTs, σ_{eff}, (commonly approximated as a half of transformation stress hysteresis) decays over time,

$$\frac{\partial(\sigma_{\mathrm{eff}}-\sigma_{\mu})}{\partial t}=-E_{\mathrm{A}}\exp\left\{\ln\dot{\varepsilon}_0-\frac{Q}{k_{\mathrm{B}}T}\left[1-\left(\frac{\sigma_{\mathrm{eff}}-\sigma_{\mu}}{\sigma_{\mathrm{TA}}}\right)^{p}\right]^{q}\right\} \tag{1}$$

where σ_{μ} and σ_{TA} represent the athermal component and thermal activation offset at 0 K of σ_{eff}, respectively; Q the activation energy; k_{B} the Boltzmann constant;ε_0 a pre-exponential factor; E_{A} the elastic modulus

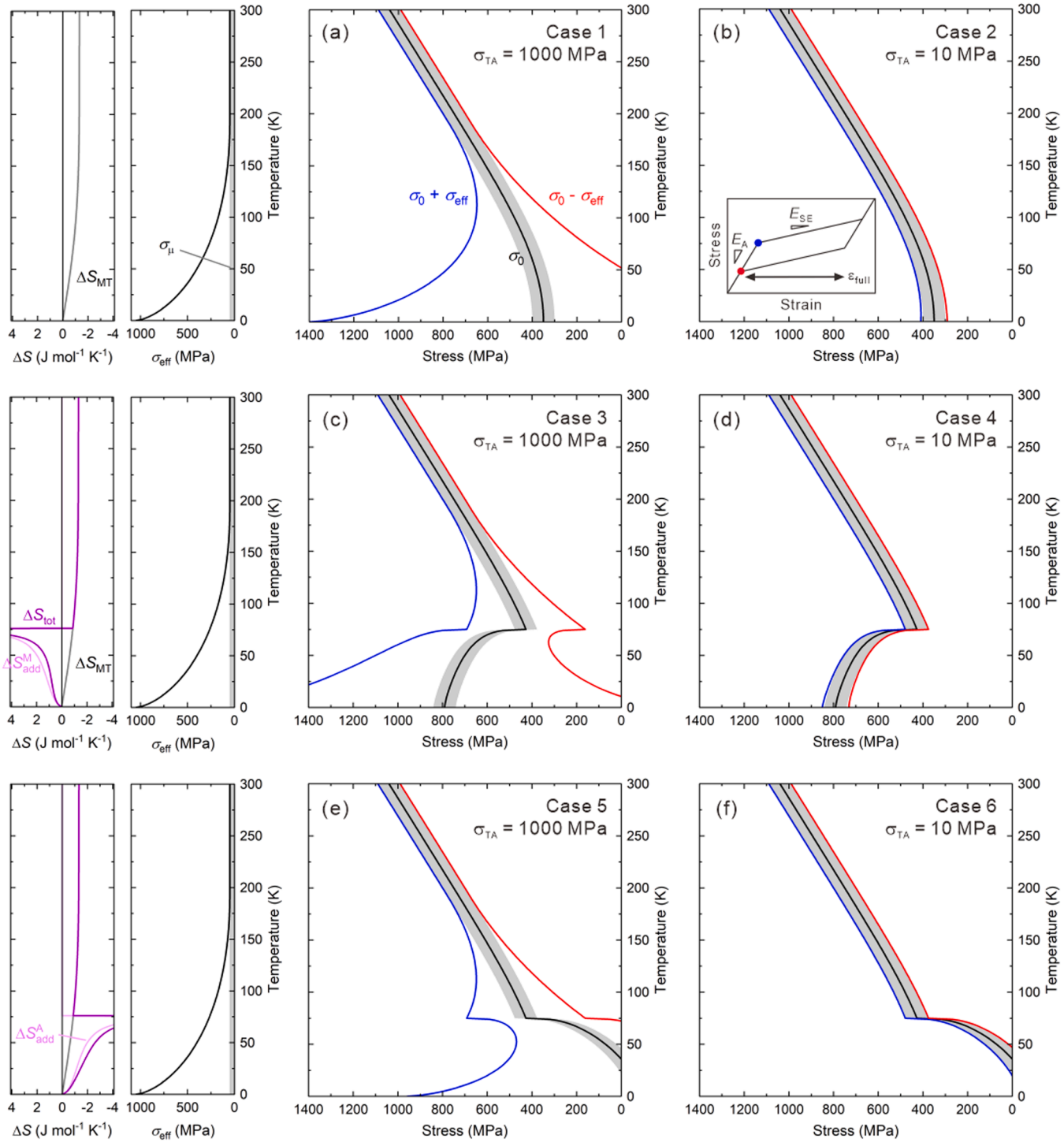

Fig. 1. Experimentally accessible phase diagrams for the model cases considered in this study. The temperature functions of entropy change and effective stress are presented in their left panels. The additional entropy change is absent in cases (a) 1 and (b) 2, appended on the martensite phase in cases (c) 3 and (d) 4, and appended on the austenite phase in cases (e) 5 and (f) 6, respectively. Other parameters are uniquely set as follows: $\sigma_{\mu}=50$ MPa, $Q=0.47$ eV, $E_{\mathrm{A}}=50$ GPa, ln $\varepsilon_0=20.5$, $\sigma_0=350$ at 0 K for cases 1 and 2.

of the austenite phase; t time; T temperature; and p and q are fitting parameters that characterize the curvature of the temperature and strain-rate dependence of σ_{eff}. It is empirically known that the combination of $p = 1/2$ and $q = 3/2$ is the most reproducible [21–23]. This equation was derived by integrating two concepts of thermal activation [24] and viscous dynamics [25]; their mathematical expressions are

$$\sigma_{\mathrm{eff}} = \sigma_{\mu} + \sigma_{\mathrm{TA}} \left[1 - \left\{ \frac{k_{\mathrm{B}} T}{Q} \ln\left(\frac{\dot{\varepsilon}_0}{\dot{\varepsilon}_{\mathrm{SE}}} \right) \right\}^{1/q} \right]^{1/p} \tag{2}$$

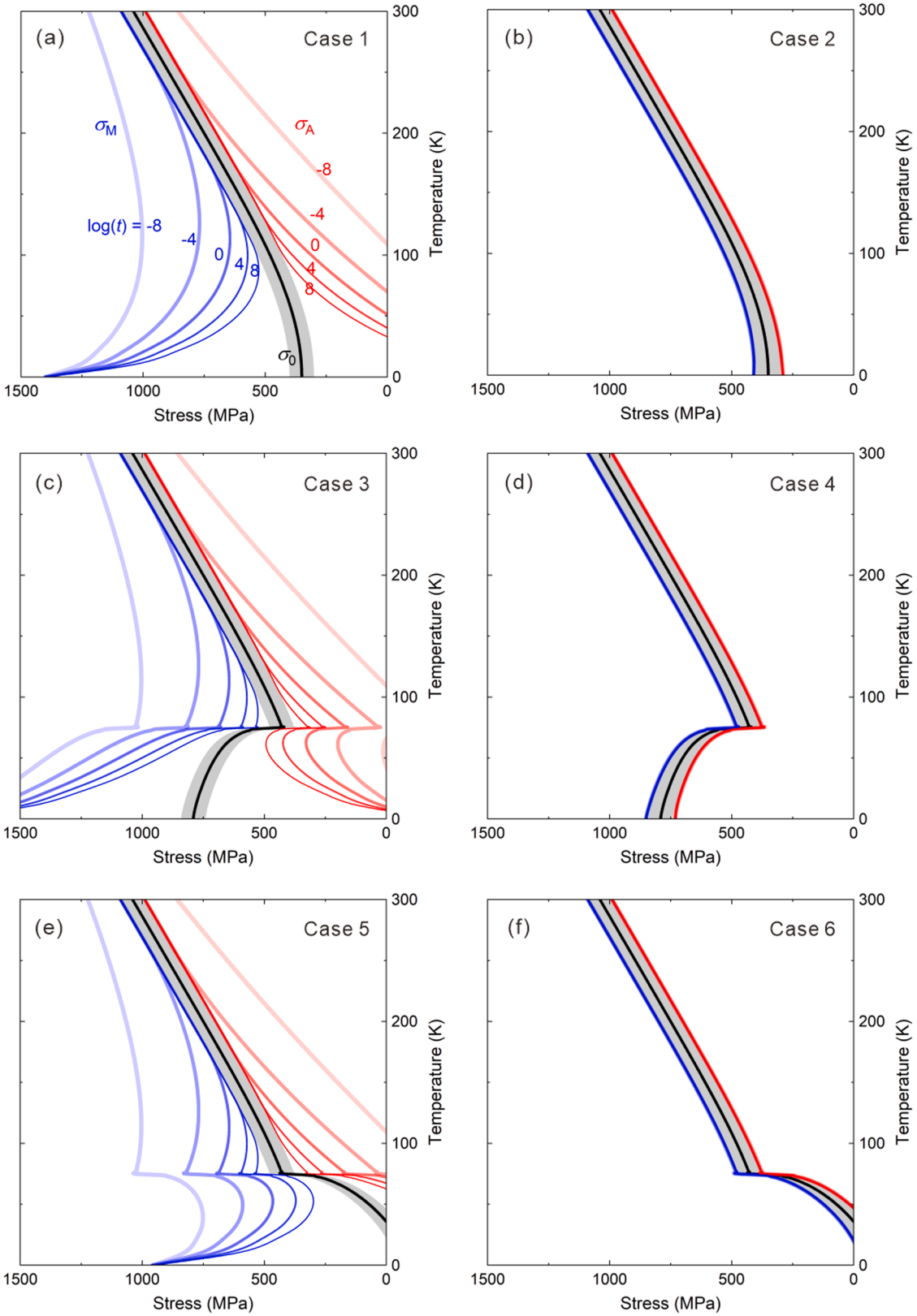

Fig. 2. Time-dependent dynamic phase diagrams for cases (a) 1 to (f) 6.

and

$$\varepsilon = \varepsilon_e + \varepsilon_{SE} \tag{3}$$

where ε, ε_e, and ε_{SE} represent the total strain, austenitic elastic strain, and superelastic strain, respectively, and $\dot{\varepsilon}_{SE}$ is the superelastic strain rate.

Another important factor dictating MT dynamics is thermodynamic equilibrium. The temperature dependence of the equilibrium stress σ_0 shapes the backbone of the phase diagram and makes the isothermal *TTT* (*time–temperature–transformation*) diagram non-reciprocal between forward and reverse MT pathways [20]. The curvature varies in obedience to the Clausius-Clapeyron relation; for stress-induced MT, σ_0 follows

$$\frac{\partial \sigma_0}{\partial T} = -\frac{\Delta S_{tot}}{\varepsilon_{SE} \cdot V_M} \tag{4}$$

where V_M and ΔS_{tot} represent molar volume and total entropy change, respectively [11]. Herein, $\Delta S_{tot} = \Delta S_{MT} + \Delta S_{add}^{A/M}$, where ΔS_{MT} is the transformation entropy change and $\Delta S_{add}^{A/M}$ is the additional entropy change appended to the austenite (A) or martensite (M) phase. Entropy change due to magnetic transitions is a typical example of $\Delta S_{add}^{A/M}$.

As demonstrated in previous studies (see, e.g., refs. 21, 22, and 24), the temperature dependence of σ_0 and σ_{eff} can be determined by obtaining superelastic stress-strain curves at various temperatures and strain rates. Most of the parameters in Eq. 1 can be extracted by fitting with Eqs. 2 and 4. Then the time-dependent MT evolution can be evaluated by solving Eq. 1, which results in deriving the *time--temperature-transformation* (*TTT*) diagrams at any holding stress. The concept of viscosuperelasticity has offered a comprehensive interpretation of various low-temperature anomalous dynamics such as non-reciprocal isothermal dynamics, kinetic arrest, and non-ergodicity in the anelastic strain as manifestations of thermal activation of MTs [20]. It should be mentioned that this result implies that the dynamics of stress-induced MTs can be adequately dictated by growth dynamics alone without considering nucleation.

This study aims to generalize the concept of viscosuperelasticity by applying it to various cases of combinations of thermodynamic and kinetic conditions. For various exceptional behaviors at low temperatures, this study demonstrates that these can be interpreted with the concept of viscosuperelasticity. Moreover, undiscovered exceptional dynamics are also predicted to occur.

2. Models

In light of the purpose of this study, some parameters that characterize the phase diagram are given *a priori*. Six representative cases presented in Fig. 1 are considered in this study, wherein the numerical values of the parameters are provided in this figure and its caption. From a kinetic point of view, two cases are assumed: one with a pronounced hysteresis broadening (cases 1, 3, and 5) with $\sigma_{TA} = 1000$ MPa and the other with a less pronounced hysteresis broadening (cases 2, 4, and 6) with $\sigma_{TA} = 10$ MPa. From a thermodynamic point of view, three cases are assumed: without the additional entropy change (cases 1 and 2), with ΔS_{add}^{M} (cases 3 and 4), and with ΔS_{add}^{A} (cases 5 and 6). Therefore, a total of six phase diagrams are considered here.

The temperature functions of the entropy changes, σ_{eff}, and σ_μ are given in the left panels of their phase diagrams in Fig. 1. It should be mentioned that ΔS_{MT} is replicated as a temperature function that mimics the Debye model of lattice specific heat and $\Delta S_{add}^{A/M}$ is modeled by well-defined magnetic entropy change due to a 2nd-order magnetic transition. The transition temperature T_C of the 2nd-order transition is set to 75 K. Case 1 mimics the phase diagram of the Ti–Ni and Ni–based Heusler systems [21,22], case 2 does the Cu–Al–Mn system [12], and case 4 does the Co–based Heusler system [26], respectively. It has been demonstrated that the temperature dependence of superelastic property can be designed by varying T_C and $\Delta S_{add}^{A/M}$ [27]. The superelastic stress-strain curve simply assumes a parallelogram shape, as shown in the inset of Fig. 1b, with the superelastic hardening ratio $E_{SE} = 2.0$ GPa and the full superelastic strain $\varepsilon_{full} = 0.1$.

3. Results and discussion

Using the given parameters, the time-dependent hysteresis changes can be derived by solving Eq. 1. The impact of time on stress hysteresis is highlighted in Fig. 2. Note that these phase diagrams are for $V_M = 0$, that is, the blue and red lines are drawn for the onset and offset of stress-induced forward and reverse MTs. Similar phase diagrams can be derived for any V_M by shifting σ_0 by $\Delta\sigma_0$ laterally using the relations $V_M = \varepsilon_{SE}/\varepsilon_{full}$ and $\Delta\sigma_0 = \varepsilon_{SE} \cdot E_{SE}$. When the thermal activation contribution is significant (cases 1, 3, and 5), the hysteresis decays dramatically over time. This explicitly demonstrates the influence of thermal activation.

If the time-dependent dynamic phase diagrams for $0 \le V_M \le 1$ are cross-sectioned at a certain holding stress σ_h, one can get the *time-temperature-transformation* (*TTT*) diagrams. Several σ_h sections for forward and reverse isothermal MTs are shown in Fig. 3. For cases 2, 4, and 6 where thermal activation is negligible, almost no time dependence can be found in their *TTT* diagrams. This is a reasonable consequence in light of the time-dependent nature of thermal activation. For cases 1, 3, and 5, where thermal activation is significant, on the contrary, time-dependent curvature is visible in both the forward and reverse *TTT* diagrams. As demonstrated in ref. 20, this curvature is essentially outlined by the full C-shaped curve in the forward *TTT* diagrams and by the underside of the C-shaped curve in the reverse *TTT* diagrams, respectively. This non-reciprocity between forward and reverse MT paths originates from the curvature of σ_0, which forms the backbone of their phase diagrams.

In cases 3, 4, 5, and 6, their σ_0 backbones are reshaped by $\Delta S_{add}^{A/M}$, which modulates the corresponding *TTT* diagrams below the T_C. When ΔS_{add}^{M} exists (cases 3 and 4), the phase stability of austenite is restored. This results in the C-shaped contours showing the reverse MT in the reverse *TTT* diagram of case 3 and the austenite-stabilized band in the reverse *TTT* diagram of case 4. More importantly, the same band appears in the forward *TTT* diagram of case 4 due to the intrusion of the austenite phase region. When ΔS_{add}^{A} exists (cases 5 and 6), the phase stability of martensite is enforced. This tendency is manifested in the forward *TTT* diagram of case 5 as additional C-shaped contours, resulting in dual nose temperatures (see the inset of Fig. 3e).

Since most experiments are performed under dynamic temperature sweeps, showing *TTT* diagrams is still not instructive to compare with experimental facts. Then, let the *TTT* diagrams convert to the CCT/CHT (continuous cooling/heating transformation) diagrams. Define $\mathbf{r} = (T, t)$ (in dimensionless units) as the temperature sweep route and consider the following three cooling/heating routes:

$\mathbf{r}_{FC}$: Continuous cooling from 300 K with $\sigma_h = 700$ MPa (hereafter referred to as FC)

$\mathbf{r}_{ZFC\text{-}FH}$: Continuous heating from 0 K with $\sigma_h = 700$ MPa after zero-field ($\sigma_h = 0$) cooling (ZFC-FH)

$\mathbf{r}_{FC\text{-}FH}$: Continuous heating from 0 K with $\sigma_h = 500$ MPa after field (large σ_h enough to reach $V_M = 1$ at 0 K) cooling (FC-FH)

The basic protocol for this conversion is very simple: integrating the V_M change along $\mathbf{r}$ at various cooling/heating rates on the *TTT* diagrams and mapping V_M on the CCT/CHT matrices. Yet, due to the hysteretic nature of MT, the calculations are divided for the crossover between the sweeping temperature and some characteristic temperatures.

The V_M change along $\mathbf{r}_{FC}$ can be derived as follows:

when $T_\mu^M < T$, $\frac{\partial V_M(\mathbf{r}_{FC})}{\partial t} = \frac{\partial V_M(\mathbf{r}_{FC})}{\partial T} = 0$,

when $T_\mu^{M'} < T \le T_\mu^M$, for the forward *TTT* diagram,

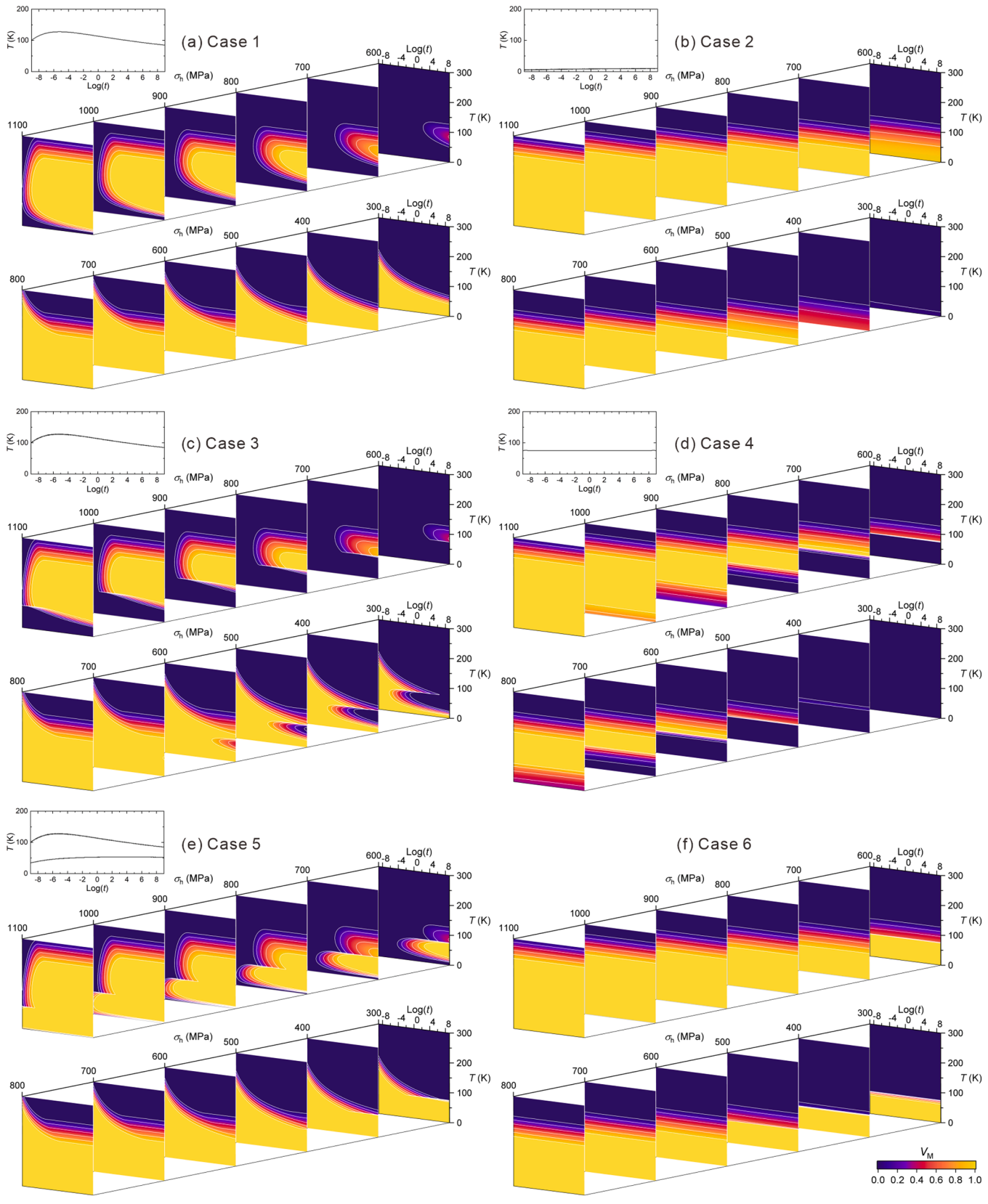

Fig. 3. Stress-sectioned *TTT* diagrams for isothermal (upper) forward and (lower) reverse MTs for cases (a) 1 to (f) 6. White contour lines are drawn for V_M interval of 0.2. The top left panels show the nose temperature of the isothermal forward MT as a function of time.

$$V_M(\mathbf{r}_{FC}) = V_M(\mathbf{r}^0_{FC}) + \int_{\mathbf{r}_{FC}} \frac{\partial V_M(\mathbf{r}_{FC})}{\partial t} dt + \Psi \int_{\mathbf{r}_{FC}} \frac{\partial V_M(\mathbf{r}_{FC})}{\partial T} dT$$

where

$$\Psi = \begin{cases} -1 & (\text{if } \partial V_M(\mathbf{r}_{FC})/\partial T < 0) \\ 0 & (\text{if } \partial V_M(\mathbf{r}_{FC})/\partial T \geq 0) \end{cases} \quad (5)$$

when $T^{A'}_{\mu} < T \leq T^{M'}_{\mu}$, $\frac{\partial V_M(\mathbf{r}_{FC})}{\partial t} = \frac{\partial V_M(\mathbf{r}_{FC})}{\partial T} = 0$,
and when $T \leq T^{A'}_{\mu}$, for the reverse *TTT* diagram,

$$V_M(\mathbf{r}_{FC}) = V_M\left(T^{A'}_{\mu}, t^{A'}_{\mu}\right) + \int_{\mathbf{r}_{FC}} \frac{\partial V_M(\mathbf{r}_{FC})}{\partial t} dt + \Psi' \int_{\mathbf{r}_{FC}} \frac{\partial V_M(\mathbf{r}_{FC})}{\partial T} dT$$

where

$$\Psi' = \begin{cases} 0 & (\text{if } \partial V_M(\mathbf{r}_{FC})/\partial T < 0) \\ -1 & (\text{if } \partial V_M(\mathbf{r}_{FC})/\partial T \geq 0) \end{cases} \quad (6)$$

The V_M change along $\mathbf{r}_{ZFC\text{-}FH}$ can be derived as follows:
when $T \leq T^{M'}_{\mu}$, $V_M = 0$,
when $T^{M'}_{\mu} < T \leq T^{M}_{\mu}$, for the forward *TTT* diagram,

$$V_M(\mathbf{r}_{ZFC-FH}) = V_M(\mathbf{r}^0_{ZFC-FH}) + \int_{\mathbf{r}_{ZFC-FH}} \frac{\partial V_M(\mathbf{r}_{ZFC-FH})}{\partial t} dt + \Phi \int_{\mathbf{r}_{ZFC-FH}} \frac{\partial V_M(\mathbf{r}_{ZFC-FH})}{\partial T} dT$$

where

$$\Phi = \begin{cases} 1 & (\text{if } \partial V_M(\mathbf{r}_{ZFC-FH})/\partial T \geq 0) \\ 0 & (\text{if } \partial V_M(\mathbf{r}_{ZFC-FH})/\partial T < 0) \end{cases} \quad (7)$$

when $T^{M}_{\mu} < T \leq T^{A}_{\mu}$, $\frac{\partial V_M(\mathbf{r}_{ZFC-FH})}{\partial t} = \frac{\partial V_M(\mathbf{r}_{ZFC-FH})}{\partial T} = 0$,
and when $T^{A}_{\mu} < T$, for the reverse *TTT* diagram,

$$V_M(\mathbf{r}_{ZFC-FH}) = V_M\left(T^{A}_{\mu}, t^{A}_{\mu}\right) + \int_{\mathbf{r}_{ZFC-FH}} \frac{\partial V_M(\mathbf{r}_{ZFC-FH})}{\partial t} dt + \Phi' \int_{\mathbf{r}_{ZFC-FH}} \frac{\partial V_M(\mathbf{r}_{ZFC-FH})}{\partial T} dT$$

where

$$\Phi' = \begin{cases} 1 & \left(\text{if } \partial V_M(\mathbf{r}_{ZFC/FC-FH})/\partial T < 0\right) \\ 0 & \left(\text{if } \partial V_M(\mathbf{r}_{ZFC/FC-FH})/\partial T \geq 0\right) \end{cases} \quad (8)$$

Finally, the V_M change along $\mathbf{r}_{FC\text{-}FH}$ can be derived as follows:
when $T \leq T^{A'}_{\mu}$, for the reverse *TTT* diagram,

$$V_M(\mathbf{r}_{FC-FH}) = V_M(\mathbf{r}^0_{FC-FH}) + \int_{\mathbf{r}_{FC-FH}} \frac{\partial V_M(\mathbf{r}_{FC-FH})}{\partial t} dt + \Omega \int_{\mathbf{r}_{FC-FH}} \frac{\partial V_M(\mathbf{r}_{FC-FH})}{\partial T} dT,$$

where

$$\Omega = \begin{cases} 1 & (\text{if } \partial V_M(\mathbf{r}_{FC-FH})/\partial T < 0) \\ 0 & (\text{if } \partial V_M(\mathbf{r}_{FC-FH})/\partial T \geq 0) \end{cases} \quad (9)$$

when $T^{A'}_{\mu} < T \leq T^{M'}_{\mu}$, $\frac{\partial V_M(\mathbf{r}_{FC-FH})}{\partial t} = \frac{\partial V_M(\mathbf{r}_{FC-FH})}{\partial T} = 0$,
when $T^{M'}_{\mu} < T \leq T^{M}_{\mu}$, for the forward *TTT* diagram,

$$V_M(\mathbf{r}_{FC-FH}) = V_M\left(T^{M'}_{\mu}, t^{M'}_{\mu}\right) + \int_{\mathbf{r}_{FC-FH}} \frac{\partial V_M(\mathbf{r}_{FC-FH})}{\partial t} dt + \Omega' \int_{\mathbf{r}_{FC-FH}} \frac{\partial V_M(\mathbf{r}_{FC-FH})}{\partial T} dT$$

where

$$\Omega' = \begin{cases} 1 & (\text{if } \partial V_M(\mathbf{r}_{ZFC-FH})/\partial T \geq 0) \\ 0 & (\text{if } \partial V_M(\mathbf{r}_{ZFC-FH})/\partial T < 0) \end{cases} \quad (10)$$

when $T^{M}_{\mu} < T \leq T^{A}_{\mu}$, $\frac{\partial V_M(\mathbf{r}_{FC-FH})}{\partial t} = \frac{\partial V_M(\mathbf{r}_{FC-FH})}{\partial T} = 0$,
and when $T^{A}_{\mu} < T$, for the reverse *TTT* diagram,

$$V_M(\mathbf{r}_{FC-FH}) = V_M\left(T^{A}_{\mu}, t^{A}_{\mu}\right) + \int_{\mathbf{r}_{FC-FH}} \frac{\partial V_M(\mathbf{r}_{FC-FH})}{\partial t} dt + \Omega'' \int_{\mathbf{r}_{FC-FH}} \frac{\partial V_M(\mathbf{r}_{FC-FH})}{\partial T} dT$$

where

$$\Omega'' = \begin{cases} 1 & (\text{if } \partial V_M(\mathbf{r}_{FC-FH})/\partial T < 0) \\ 0 & (\text{if } \partial V_M(\mathbf{r}_{FC-FH})/\partial T \geq 0) \end{cases} \quad (11)$$

$\mathbf{r}^0_{FC}$, $\mathbf{r}^0_{FC\text{-}FH}$, and $\mathbf{r}^0_{ZFC\text{-}FH}$ are the starting point of these calculations and herein set to $\mathbf{r}^0_{FC} = (300, 1)$, and $\mathbf{r}^0_{FC\text{-}FH} = \mathbf{r}^0_{ZFC\text{-}FH} = (0, 1)$, respectively. T^{M}_{μ} and t^{M}_{μ}, and T^{A}_{μ} and t^{A}_{μ} are the temperature and time at which $\sigma_h = \sigma_0 + \sigma_\mu$ and $\sigma_h = \sigma_0 - \sigma_\mu$ are satisfied, respectively. In cases 3 and 4, there may be two temperatures satisfying $\sigma_h = \sigma_0 + \sigma_\mu$ and $\sigma_h = \sigma_0 - \sigma_\mu$ upon continuous temperature sweep, the lower temperatures of which are denoted by "M'" and "A'". For the other cases, since M' and A' points are missing, calculate the above equations as M' and A' → 0. It is important to note that T^{M}_{μ}, T^{A}_{μ}, $T^{M'}_{\mu}$, and $T^{A'}_{\mu}$ are V_M-dependent.

Eqs. 5–11 were calculated for $\mathbf{r}_{FC}$, $\mathbf{r}_{ZFC\text{-}FH}$, and $\mathbf{r}_{FC\text{-}FH}$ at various cooling/heating rates ranging from 10^{-8} to 10^{3} K/s. The derived CCT and CHT diagrams for $\mathbf{r}_{FC}$, $\mathbf{r}_{ZFC\text{-}FH}$, and $\mathbf{r}_{FC\text{-}FH}$ for all model cases are presented in Fig. 4. It is a reasonable consequence that the CCT and CHT diagrams for cases 2, 4, and 6 are almost time-independent because there is little room to thermally activate the MTs. Comparing the CCT and CHT diagrams for $\mathbf{r}_{FC}$ and $\mathbf{r}_{ZFC\text{-}FH}$ at $\sigma_h = 700$ MPa, the contours in the CHT diagrams for $\mathbf{r}_{ZFC\text{-}FH}$ are somewhat shifted upward compared to those in the CCT diagrams for $\mathbf{r}_{FC}$, and the contours in the CCT diagrams for $\mathbf{r}_{FC}$ tends to trail to 0 K. These behaviors are ascribed to the hysteretic nature of MT. As a typical example, the variation of V_M along the gray and red lines overlaid onto Fig. 4a is extracted in Fig. 5a. The hysteretic behavior observed in the temperature range of 100–200 K reflects the hysteresis of MT, and the blocking below 100 K results from the kinetic arrest of forward MT. These behaviors have been experimentally confirmed. This result is a simple answer to the temperature history dependence (sometimes referred to as "non-ergodicity") of V_M. The red line in Fig. 5a indicates the occurrence of heating-induced forward MT. This is indeed confirmed to occur [20]. Exceptional behaviors are also found in cases 3 and 4; the variation of V_M along the green and blue lines overlaid onto Fig. 4c and d is shown in Fig. 5b and c, respectively. In case 3 (see Fig. 5b), a plateau appears during FH after FC. This means that the reverse MT can be arrested (or even supplanted by the forward MT) under certain special conditions. In case 4 (see Fig. 5c), the forward MT initially takes place upon FC, and the reverse MT starts to occur below the T_C. This behavior is called reentrant MT and is actually known to occur in Co–based Heusler systems [26].

As demonstrated above, the proposed algorithm, despite being based on a phenomenological model, is able to provide quantitative explanations for various manifestations involving thermally activated dynamics. This result suggests that the overall scheme seems to make sense to a large extent in dissecting the observed phenomena. Nevertheless, the present scheme is unlike other phenomenological models in some aspects and appears to be inconsistent with some experimental facts. It is important to address these points and define the capabilities of the proposed phenomenological handling.

It is generally recognized that the MTs occur as a sequence of continuously power law distributed events. One may think that this contradicts the basic assumption of the present model that σ_{eff} can be decomposed into the temperature- and strain-rate-dependent component $\sigma_{TA}\left[1 - \left\{\frac{k_B T}{Q} \ln\left(\frac{\dot{\varepsilon}_0}{\dot{\varepsilon}_{SE}}\right)\right\}^{1/q}\right]^{1/p}$ and the constant σ_μ (see Eq. 2). In this context, Q is commonly believed not to take a single value but to take a broad distribution.

Power law scalability is indeed a universal law for thermally-induced MTs [4,28,29] but is severely modified for stress-induced MTs [30]. Thermally-induced MTs largely rely on inhomogeneous nucleation events, which are likely to follow a power law scaling. However, this

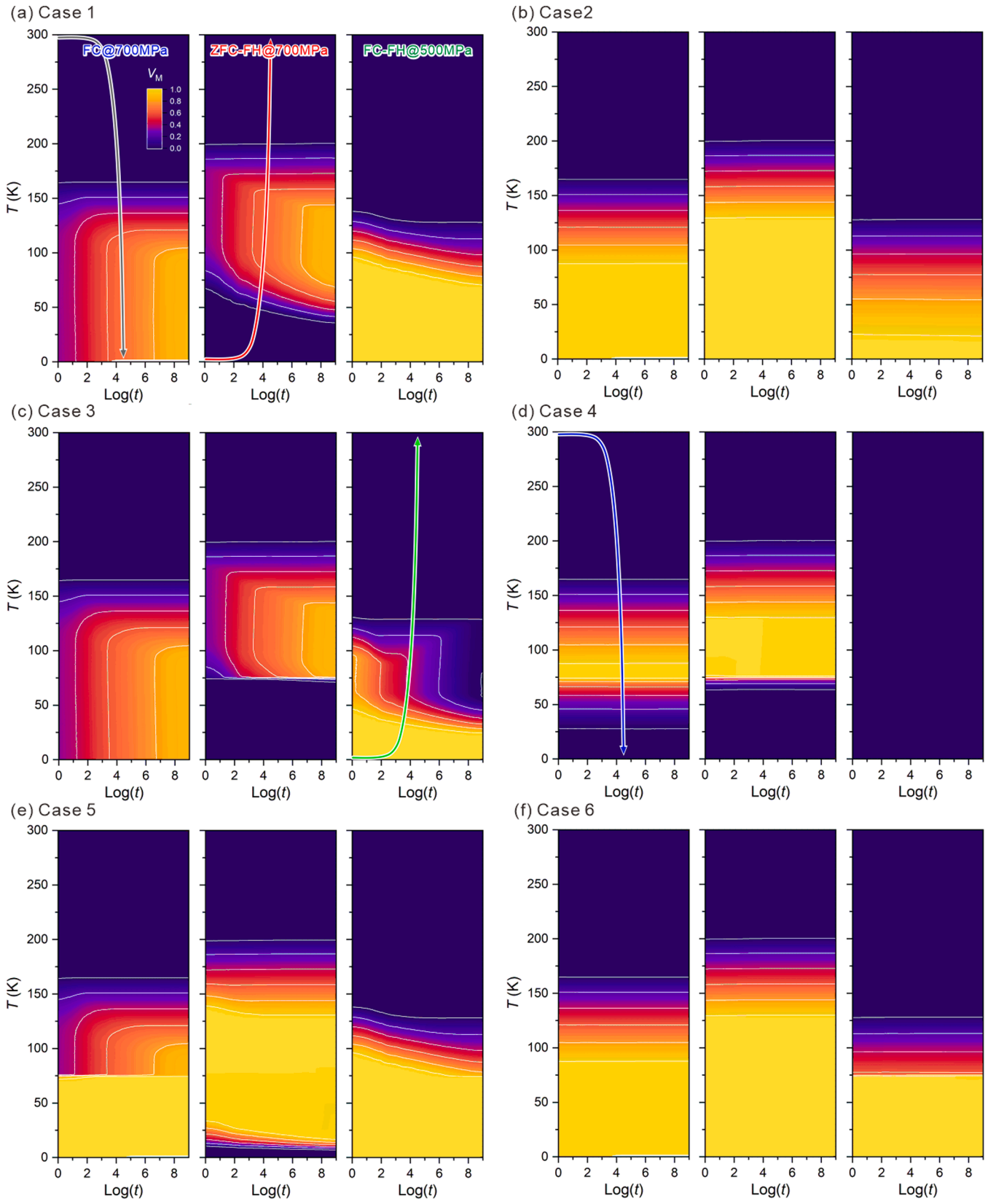

Fig. 4. CCT and CHT diagrams of the temperature sweep routes of (left panels) $\mathbf{r_{FC}}$, (center panels) $\mathbf{r_{ZFC\text{-}FH}}$, and (right panels) $\mathbf{r_{FC\text{-}FH}}$ for cases (a) 1 to (f) 6.

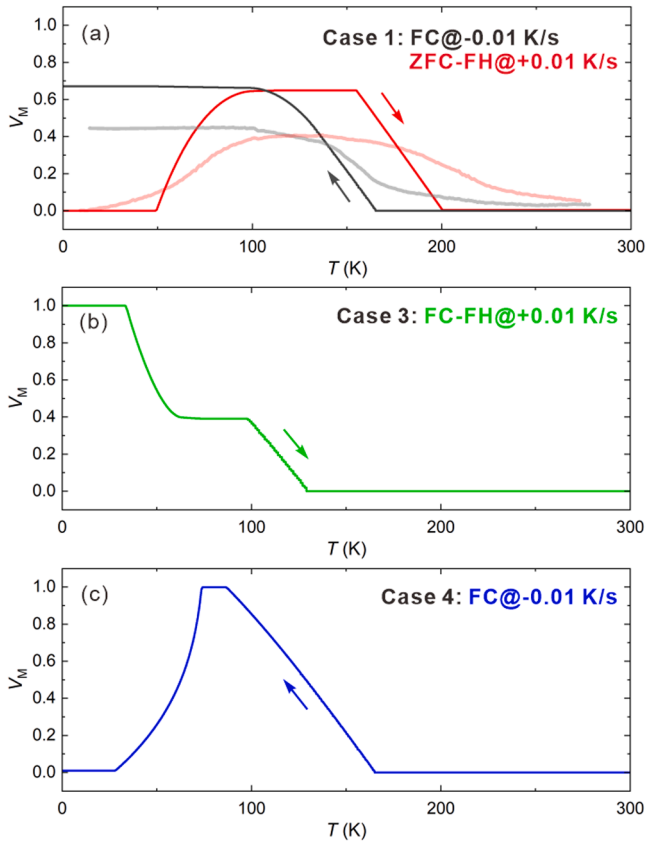

Fig. 5. Variation of V_M along the routes overlaid in Fig. 4: (a) $\mathbf{r}_{FC}$ at a rate of −0.01 K/s and $\mathbf{r}_{ZFC\text{-}FH}$ at 0.01 K/s for case 1, (b) $\mathbf{r}_{FC\text{-}FH}$ at 0.01 K/s for case 3, and (c) $\mathbf{r}_{FC}$ at −0.01 K/s for case 4. In (a), experimental results analyzed from the reference data [21] are also shown in transparent color, where the demonstrated sweep rate is 4.8×10^{-3} K/s and $\sigma_h = 750$ MPa.

event becomes less likely to occur and is supplanted by continuous growth through mechanical cycling in the case of stress-induced MTs. Indeed, Nataf [30] reported for a Ni-rich Ti-Ni alloy that the acoustic emission (AE) activity dramatically decays after a few superelastic cycles, and its energies become undetectably small (< 20 aJ) although still exhibiting typical Luders-like microstructures and superelastic macroscopic responses. The author assumes that the simple form and the single-Q approximation of the proposed model reflect two elementary growth processes that shape the macroscopic growth of variants: the kink-pair formation and its glide along the habit plane surface, both energy scales would be undetectable by AE.

In analogous to the movement of dislocations, the kink-pair formation is likely to be thermally activated. Therefore, the temperature- and strain-rate-dependent hysteresis component is manidfested by the short-range-interacting kink-pair formations, which are ideally stipulated by a unique Q value. The constant σ_μ may correspond to the long-range glides of the kinks and should have less dependence on temperature and strain rate. The uniqueness of the activation energy has also been reported for the growth dynamics of a different 1st-order phase transformation exhibiting hysteresis broadening [31]. The author emphasizes that the concept of viscosuperelasticity stems from the phenomenology of growth dynamics rather than nucleation. Experimental validations of these assumptions are underway.

4. Conclusions

In summary, the impact of thermal activation is studied for some representative model cases of thermodynamic and kinetic conditions. Low-temperature MT dynamics are not straightforward without the scale of time because thermal activation holds time dependence. This complexity can be mathematically resolved by integrating the phenomenology of viscosity and thermal activation, the concept of which is herein termed viscosuperelasticity. The impact of viscosuperelasticity is visualized in the presentations of *TTT*, CCT, and CHT diagrams, making it possible to interpret tricky behaviors often observed at low temperatures or even predict undiscovered behaviors. This study guides the way to manifest the impact of time from experimentally accessible MT behaviors and provides a systematic understanding of low-temperature MT dynamics. The findings will help understand and design the low-temperature functionalities of MTs.

Prime novelty statement

A phenomenological kinetic theory of the growth dynamics of thermoelastic martensitic transformations (MT) is developed based on the concept of thermal activation. The derived mathematical form comprehensively uncovers the impact of time on the dynamics for various combinations of kinetic and thermodynamic conditions for MT-hosting alloy systems. This concept enables seemingly strange low-temperature behaviors to be explained as manifestations of thermal activation. Furthermore, undiscovered exceptional dynamics are also predicted to occur. This study guides the way to manifest the impact of time from experimentally accessible MT behaviors and provides a systematic understanding of low-temperature MT dynamics. Since the framework of this theory does not include any prerequisite for MTs, the concept has the potential capability to explain the thermally activated dynamics of other kinds of phase transformations. Therefore, I believe that this manuscript will have a broader impact on the materials science community.

Declaration of Competing Interest

The authors declare that they have no known competing financial interests or personal relationships that could have appeared to influence the work reported in this paper.

Data availability

Data will be made available on request.

Acknowledgments

This study was supported by the Mizuho Foundation for the Promotion of Sciences, Kyoto University Foundation, JST PRESTO (Grant No. JPMJPR22Q6), and JSPS KAKENHI (Grants No. 23K04366, No. 19H02418, and No. 19K22052).

References

[1] G.V. Kurdjumov, O.P. Maksimova, Kinetics of austeniteto-martensite transformation at low temperatures, Dokl. Akad. Nauk SSSR 61 (1948) 83–86.
[2] G.V. Kurdjumov, O.P. Maksimova, Work required in the formation of martensite nuclei, Dokl. Akad. Nauk SSSR 73 (1950) 95–98.
[3] E.S. Machlin, M. Cohen, Isothermal mode of the martensitic transformation, JOM 4 (1952) 489–500.
[4] R.E. Cech, J.H. Hollomon, Rate of formation of isothermal martensite in Fe–Ni–Mn, Trans. Metall. Soc. AIME 197 (1953) 685–689.
[5] J.C. Fisher, Application of nucleation theory to isothermal martensite, Acta Met. 1 (1953) 32–35.
[6] C.H. Shih, B.L. Averbach, M. Cohen, Some characteristics of the isothermal martensitic transformation, Trans. Metall. Soc. AIME 203 (1955) 183–187.
[7] V. Raghavan, Martensite, ASM International, Materials Park, Ohio, 1992.
[8] T. Kakeshita, J. Katsuyama, T. Fukuda, T. Saburi, Time-dependent nature of displacive transformations in Fe–Ni and Fe–Ni–Mn alloys under magnetic field and hydrostatic pressure, Mater. Sci. Eng. A 312 (2001) 219–226.
[9] F.J. Romero, J. Manchado, J.M. Martín-Olalla, M.C. Gallardo, E.K.H. Salje, Dynamic heat flux experiments in Cu67.64Zn16.71Al15.65: Separating the time scales of fast and ultra-slow kinetic processes in martensitic transformations, Appl. Phys. Lett. 99 (2011) 011906.

[10] J. Xia, X. Xu, A. Miyake, Y. Kimura, T. Omori, M. Tokunaga, R. Kainuma, Shap. Mem. Superelasticity 3 (2017) 467–475.
[11] K. Otsuka, C.M. Wayman, Shape Memory Materials, Cambridge University Press, UK, 1998.
[12] K. Niitsu, Y. Kimura, T. Omori, R. Kainuma, Cryogenic superelasticity with large elastocaloric effect, NPG Asia Mater. 10 (2018) e457.
[13] L. Kaufman, M. Cohen, Thermodynamics and kinetics of martensitic transformations, Prog. Met. Phys. 7 (1958) 165–246.
[14] S. Kajiwara, Morphology and crystallography of the isothermal martensite transformation in Fe—Ni—Mn alloys, Philos. Mag. 43 (1981) 1483–1503.
[15] T. Kikuchi, S. Kajiwara, HVEM in situ observation of isothermal martensitic transformation under applied stress, Trans. Jpn. Inst. Met. 26 (1985) 861–868.
[16] G. Ghosh, V. Raghavan, The kinetics of isothermal martensitic transformation in an Fe–23.2wt%Ni–2.8wt%Mn alloy, Mater. Sci. Eng. A 80 (1986) 65–74.
[17] T. Kakeshita, K. Kuroiwa, K. Shimizu, T. Ikeda, A. Yamagishi, M. Date, A new model explainable for both the athermal and isothermal natures of martensitic transformations in Fe–Ni–Mn alloys, Mater. Trans. JIM 34 (1993) 423–428.
[18] G. Ghosh, G.B. Olson, Kinetics of FCC → BCC heterogeneous martensitic nucleation—I. The critical driving force for athermal nucleation, Acta Metall. Mater. 42 (1994) 3361–3370.
[19] G. Ghosh, G.B. Olson, Kinetics of F.c.c. → b.c.c. heterogeneous martensitic nucleation—II. Thermal activation, Acta Metall. Mater. 42 (1994) 3371–3379.
[20] K. Niitsu, Y. Yano, R. Kainuma, H. Inui, Viscosity of superelasticity: A comprehensive interpretation of nonreciprocal isothermal dynamics, kinetic arrest, and nonergodic anelastic strain based on thermal activation of martensitic transformations, Phys. Rev. B 108 (2023) 134103.
[21] K. Niitsu, T. Omori, R. Kainuma, Stress-induced transformation behaviors at low temperatures in Ti–51.8 Ni (at%) shape memory alloy, Appl. Phys. Lett. 102 (2013) 231915.
[22] K. Niitsu, X. Xu, R.Y. Umetsu, R. Kainuma, Stress-induced transformations at low temperatures in a $Ni_{45}Co_5Mn_{36}In_{14}$ metamagnetic shape memory alloy, Appl. Phys. Lett. 103 (2013) 242406.
[23] R.Y. Umetsu, X. Xu, R. Kainuma, NiMn-based metamagnetic shape memory alloys, Scr. Mater. 116 (2016) 1–6.
[24] K. Niitsu, H. Date, R. Kainuma, Thermal activation of stress-induced martensitic transformation in Ni–rich Ti–Ni alloysm, Scr. Mater. 186 (2020) 263–267.
[25] D. François, A. Pineau, A. Zaoui, Viscoplasticity, Damage, Fracture and Contact Mechanics, Mechanical Behaviour of Materials II, Kluwer Academic Publishers, Dordrecht, 1993.
[26] X. Xu, T. Omori, M. Nagasako, A. Okubo, R.Y. Umetsu, T. Kanomata, K. Ishida, R. Kainuma, Cooling-induced shape memory effect and inverse temperature dependence of superelastic stress in Co2Cr(Ga,Si) ferromagnetic Heusler alloys, Appl. Phys. Lett. 103 (2013) 1641040.
[27] J. Xia, Y. Noguchi, X. Xu, T. Odaira, Y. Kimura, M. Nagasako, T. Omori, R. Kainuma, Iron-based superelastic alloys with near-constant critical stress temperature dependence, Science 369 (2020) 855–858.
[28] L. Carrillo, L. Mañosa, J. Ortín, A. Planes, E. Vives, Experimental evidence for universality of acoustic emission avalanche distributions during structural transitions, Phys. Rev. Lett. 81 (1998) 1889.
[29] E.K.H. Salje, K.A. Dahmen, Crackling noise in disordered materials, Annu. Rev. Condens. Matter Phys. 5 (2014) 233–254.
[30] G.F. Nataf, M. Romanini, E. Vives, B. Žužek, A. Planes, J. Tušek, X. Moya, Suppression of acoustic emission during superelastic tensile cycling of polycrystalline Ni50.4Ti49.6, Phys. Rev. Mater. 4 (2020) 093604.
[31] K. Matsuura, Y. Nishizawa, Y. Kinoshita, T. Kurumaji, A. Miyake, H. Oike, M. Tokunaga, Y. Tokura, F. Kagawa, Low-temperature hysteresis broadening emerging from domain-wall creep dynamics in a two-phase competing system, Commun. Mater. 4 (2023) 71.